3D RESEARCH **04**, 06 (2010)
10.1007/3DRes.04(2010)06

3DR REVIEW

Digital holography for 3D imaging and display in the IR range: challenges and opportunities

Anna Pelagotti • Melania Paturzo • Andrea Geltrude • Massimiliano Locatelli • Riccardo Meucci • Pasquale Poggi • Pietro Ferraro

Received: 07 October 2010 / Revised: 08 November 2010 / Accepted: 25 November 2010

Abstract In analog holography, the infrared (IR) range received quite some attention, since it could provide interesting information, not achievable otherwise. Since digital sensors in this band became recently available and affordable, also digital holography (DH) expanded its feasibility beyond the visible wavelengths. In fact, the IR range allows shorter recording distances, unparalleled larger field of view and less stringent requirements on system stability, together with some specific characteristics, like e.g. the possibility to test IR glasses or other materials transparent to IR radiation, which cannot be controlled in visible range. In this paper we review the activities which took place in this field and illustrate the results achieved, referring to the opportunities this technique offers, and the challenges it presents. We show efficient reconstructions of holograms of objects of various materials, recorded with different resolution digital thermal cameras, in various configurations, and moreover we demonstrate optical holographic display through a liquid crystal based Spatial Light Modulator which gives the chance to get direct 3D imaging and display of long IR range. Moreover we believe this opens the route toward holography in THz region.

Keywords digital holography, infrared radiation, thermal camera, infrared testing

Anna Pelagotti[1](✉) • Andrea Geltrude[1] • Massimiliano Locatelli[1] • Riccardo Meucci[1] • Pasquale Poggi[1] • Pietro Ferraro[2]
Melania Paturzo[2]
[1]CNR-INO (National Institute of Opticts), L.go E. Fermi 6, 50125 Florence, Italy
[2]CNR-INO (National Institute of Opticts , via Campi Flegrei 34, 80078 Pozzuoli
Tel.: +39-055-2308-227; Fax: +39-055-2337-755
e-mail: anna.pelagotti@ino.it

1. Introduction

The IR range was considered, from the early stage of holography, to be an important challenge, since this spectral band could open new and interesting perspectives (Prévost et al 1989, Rioux et al 1978, Beulieu et al 1978, Sakusabe et al 1971, Shigeaki et al 1971, Calixto 1988, Rioux et al 1977, Decker et al 1972, Chivian et al 1969). As a matter of fact, the use of long wavelengths reduces the sensitivity of interferometric measurements, and therefore IR holography was supposedly well suited for optical testing of aspheric optics, or to measure the optical path variation, dispensing from the use of multiple wavelengths in the visible region. It was envisaged that many materials, opaque to the visible radiation but transparent to the IR one, could be tested this way. For example, using the 10.6 μm wavelength, holography could allow inspection of infrared glasses, such as Ge, InSb, and CdHgTe, which are impossible to control in the visible and near-IR ranges (Rukman et al 1978), or could be necessary for buried integrated circuit inspections (Repetto et al 2005).

Moreover, it was known that such long wavelengths are especially appropriate to investigate plasma, since the interferometric sensitivity of interferometric measurement of electron concentrations increases with the wavelength of probing radiation (Rukman et al 1978).

Quite some efforts were devoted to find suitable recording medium for wavelengths beyond the visible range. In a comprehensive review of media for holography at 10.6 μm (Beaulieu et al 1997) more than 12 separate recording film materials were described. In the past other recording media, like liquid crystals, have been used to image IR holograms, and their visual reconstruction was proven to be feasible in the visible range, however only simple set-ups where used and tests were carried out on diffraction gratings or simple objects (Prévost et al 1989, Sakusabe et al 1971, Shigeaki et al 1971).

In the last decades, traditional film were replaced by an imaging camera even in holography and the development of solid-state image sensors, like CCD or CMOS, enabled the development of Digital Holography (Ferraro et al. 2009, Grilli et al 2001).

In order to numerically simulate the reconstruction process achievable with traditional films, a number of suitable algorithms have been developed, and to them several post processing possibilities have been added, like plane of focus adjustment (Ferraro et al 2009, Ferraro et al 2005), amplitude and phase images computing from a single hologram (Grilli et al 2001), removing aberrations (Ferraro et al 2003, Stadelmaier et al 2000), and more.

Lately, the technology of pyrocameras, and focal plane array (FPA) microbolometers offered digital sensors that do not require cryogenic cooling and have enough pixels, of appropriate size, to make the extension of DH possible also for the long IR range. In particular, the last generation microbolometers have a number of useful pixels over 300K where the pixel size has been reduced up to 25μm. The above technological progress stimulated further exploration of DH at IR long wavelengths (Allaria et al 2003, De Nicola et al 2008).

2. Experimental Section

In this paper we report investigations performed in the IR range at λ=10.6 μm. The first activities in our laboratory in this field started about 10 years ago, over time, by means of experiments, we further explored the advantages and possibilities offered by this wavelength band.

In order to test potentials of DH at long IR, we conducted trials with 6 different set-ups, and imaged objects of increasing sizes, and several different materials.

2.1 Mach-Zehnder interferometer with low resolution pixelated pyroelectric sensor, for off-axis transmission mode IR holography

In the first experiments, dating back to 2002, a conventional gas flowing CO_2 laser emitting on the P(20) line at λ=10.6 μm was employed as infrared source. The laser cavity, 82cm long, was defined by a partially reflective flat mirror (R=95%) and an out-coupling mirror (R=90%) of 3m curvature radius mounted upon a piezoelectric translator. The output laser beam was horizontally polarized by means of an intracavity ZnSe Brewster window.

The system, pumped by an electric discharge of 10mA, when the laser threshold was approximately 7mA, provided an output optical power of 190mW. The spatial profile of the laser was set on the fundamental TEM00 Gaussian mode by means of an intra-cavity iris diaphragm.

In this configuration, the laser beam was characterized by beam waist of 2.1 mm on the flat mirror and a divergence of 2 mrad. Fig. 1 shows the DH optical set-up based on a Mach–Zehnder interferometer. Two mirrors M1 and M2 and two beam splitters, BS1and BS2, were used to form the interferometer. The beam splitters were ZnSe coated windows with a diameter 50mm each.

The interferometer allowed to record the interference patterns between the two beams, the reference beam and that transmitted by the test object, on the detection plane of a pyroelectric video camera (Spiricon Pyrocam III, Model PY-III-C-A) which had a matrix of 124 × 124 pyroelectric sensor elements of $LiTaO_3$, with square pixel of 85x85 μm^2 size and center-to-center spacing of the pixels, the pixel pitch, of 100x100 μm. The pyroelectric camera allowed detection of CW infrared laser radiation by means of an internal chopper. It was connected to a personal computer to record digitized fringe patterns.

As test object a steel plate with 4 holes of 700 μm diameter was used. The steel plate was located at *Ds = 400* mm from the sensor array.

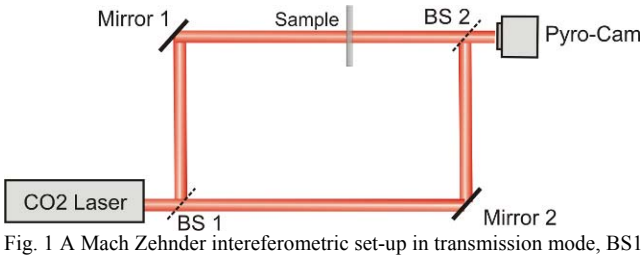

Fig. 1 A Mach Zehnder intereferometric set-up in transmission mode, BS1 and BS2 are the beam splitters

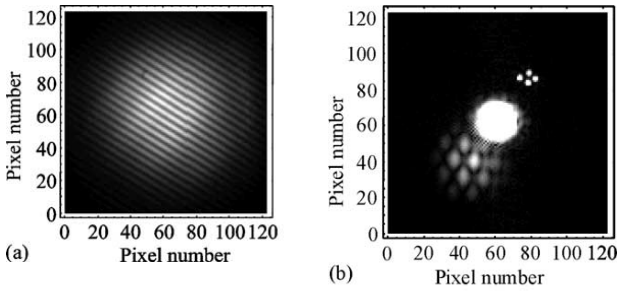

Fig. 2 (a) Digital hologram recorded with the test object (b) Amplitude reconstruction

In cases like this, and all the following ones, where the distance object camera is significantly larger than the digital recording device aperture, the numerical reconstruction of object wavefront amplitude can be performed according to the discretization of the well known Fresnel approximation of Rayleigh Sommerfeld equation. In the Fresnel approximation the reconstructed wavefield $\psi(x,y;d)$ at distance d, in the object plane, can be written in the following form

$$\psi(x,y;d)=\frac{1}{i\lambda d}\exp\left(i\frac{2\pi}{\lambda}d\right)\exp\left[i\frac{\pi}{\lambda d}\left(x^2+y^2\right)\right] \times \int_{-\infty}^{\infty}\int_{-\infty}^{\infty} I_H(\xi,\eta)R(\xi,\eta)\exp\left[i\frac{\pi}{\lambda d}\left(\xi^2+\eta^2\right)\right] \exp\left[-i\frac{2\pi}{\lambda d}(\xi x+y\eta)\right]d\xi d\eta \quad (1)$$

where $I_H(\xi,\eta)$ is the recorded and stored hologram intensity at the pyrocam array plane $\xi-\eta$ and $R(\xi,\eta)$ is the numerical model of the reference wavefield.

The discrete finite form of Eq. (1) is obtained through the pixel pitch $\Delta\xi \times \Delta\eta = 100\,\mu m \times 100\,\mu m$ of the pyrocam array and the reconstructed object field $\psi(x, y; d)$ is obtained by applying the 2-D fast Fourier transform (2DFFT) algorithm to the discrete samples of the quantity $I_H(\xi,\eta)R(\xi,\eta)\exp\left[i\pi\left(\xi^2+\eta^2\right)/\lambda d\right]$.

By the 2D-FFT algorithm, the size of the reconstruction pixel at distance d is $\Delta x \times \Delta y = d\lambda/N\Delta\xi \times d\lambda/N\Delta\eta$.

Fig. 2 shows a hologram acquired with the test object (the steel plate with holes) inserted in the interferometer arm and its amplitude reconstruction, where one hole is well visible. Fig. 3 shows the amplitude reconstruction obtained when an USAF target is used as test object.

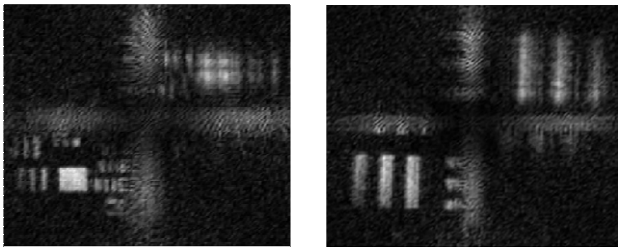

(a) (b)

Fig. 3 (a) Amplitude reconstruction of 1-2 slits (2.24 line pair/mm) of USAF test target (b) Amplitude reconstruction of 2-2 square (4.49 line pair/mm) and 0-2 square (1.12 line pair / mm) of USAF test target.

2.2 Mach-Zehnder interferometer with low resolution pixelated pyroelectric sensor, for off-axis reflection mode IR holography

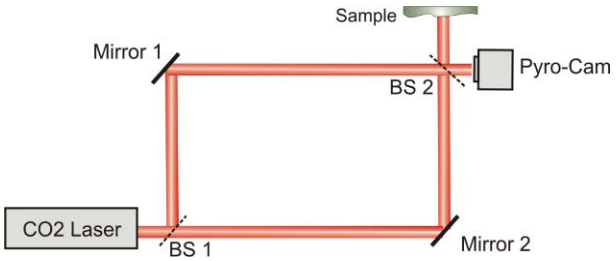

Fig. 4 A Mach Zehnder interferometric set-up in reflection mode. BS1 and BS2 are the beam splitters

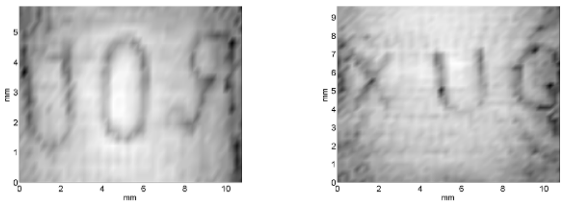

(a) (b)

Fig. 5 (a) Amplitude reconstruction of the letters “ROU”. (b) Amplitude reconstruction of the letters “XOU”.

By this configuration we demonstrated for the first time the possibility to obtain reconstructions in DH of both amplitude and phase that can be used as quantitative topographic method (De Nicola et al 2008).

We used a laser source at the same wavelength as described in 2.1, where, however, the system was set to have an optical power in the range of 500-800mW to explore a reflection mode. Fig. 4 shows the DH optical set-up based on a Mach–Zehnder interferometer in reflection configuration. The infrared beam is directed to a beam expander with magnification 2.5 × and 15 mm diameter of output beam. Two mirrors M1 and M2 and two beam splitters, BS1 (70T/30R at 450 of incidence angle) and BS2 (50T/50R at 450 of incidence angle), are used to form the interferometer. The beam splitters are ZnSe coated windows with a diameter 50mm each. As detector, the same thermal camera as in 2.1 was used.

The reflective objects used were two opaque aluminum blocks. The first one was a rectangle of size 20mm × 35mm that have letters inscribed. The letters are “UOR” and “XUO” (about 3mm - 4 mm each). The second one was a disc of radius 25.4mm which has inscribed a set of concentric circular tracks. The aluminum blocks are located at distance d=250mm from the array.

Fig. 5 shows the results of the reconstruction of the image of the letters inscribed in the first aluminum block. In fig. 5(a) the size of the reconstruction pixel is 213µm×213µm; fig. 5(b) shows the corresponding reconstructions with padding operations; The size is now 103µm×103µm, and the resolution is clearly recovered (Pelagotti et al 2009).

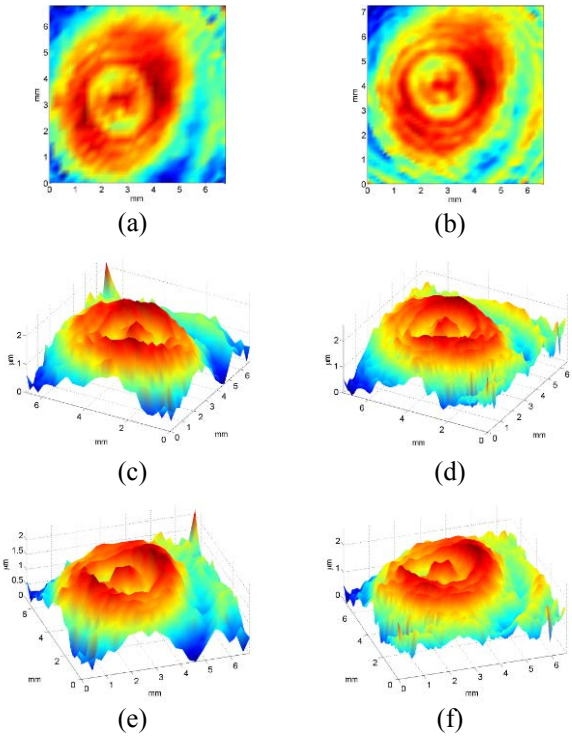

(a) (b) (c) (d) (e) (f)

Fig. 6 Phase images of aluminum disk (a) 2D reconstruction (b) 2D reconstruction with padding. (c, e) Two different perspectives of the reconstructed surface profile without padding (d, f) with zero padding.

Fig. 6 shows the phase images reconstructed form the disk shaped object. Fig. 6(a), 6(c) and 6(e) display the phase distribution of the object reconstructed without padding operation and fig. 6(b), 6(d) and 6(f) show the corresponding reconstructions with zero padding operation.

In the 3D perspectives plots of the reconstructed phase shown in fig. 6(d) and 6(f) it is noticeable that the circular-shaped tracks inscribed in the steel disk are better resolved thanks to the padding operation.

2.3 Off-axis speckle mode IR holography with a medium resolution pixelated pyroelectric sensor

In order to obtain the amplitude reconstruction of 1 and 2 euro coins, in Figure 8, a simpler interferometric reflection configuration, as shown in fig. 7, a higher resolution camera (ASi thermal camera, Miracle 110k, Thermoteknix, with 384 X 288 pixels and 35 µm pixel pitch) and a high power laser (high power CW CO2 laser, emitting at 10.6 µm, attenuated by means of a beam splitter), were used. The object was placed near the beam splitter so that the central part of the laser beam was reflected by the beam splitter towards the camera, thus working as reference beam, while the outer part was diffused by the object, thus forming the object beam. Since the beam splitter reflected only 50% of radiation impinging on it, the reference beam intensity was comparable to that of the object beam and a good fringe contrast was obtained. In this configuration it was possible to keep the camera quite near the object and obtain rather high resolution images (see also Fig. 9, where the reconstruction of a hologram of the lens mount is shown).

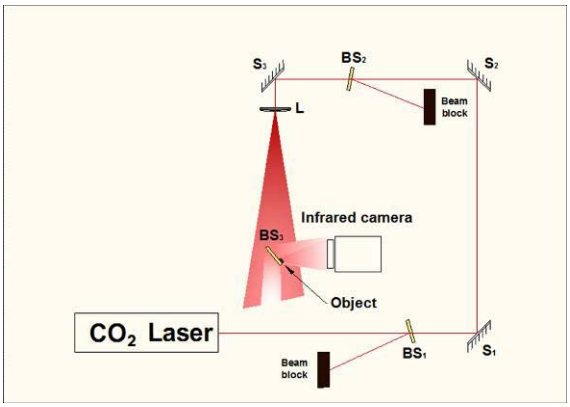

Fig. 7 Off-axis interferometric reflection set-up in reflection mode, close distance S: mirror, L: lens, BS: beam splitter

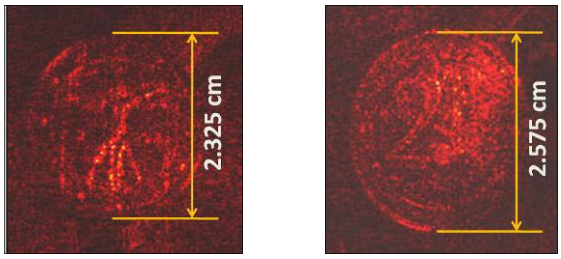

(a) (b)

Fig. 8 (a) Amplitude reconstruction of a 1 euro coin hologram recorded with the set-up described in fig. 7 (b) Amplitude reconstruction of a 2 euro coin hologram recorded with the set-up described in fig. 7

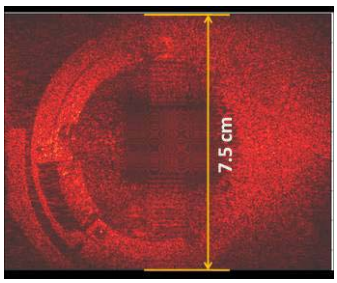

Fig. 9 Amplitude reconstructions of a lens mount hologram with the set-up described in fig. 7

2.4 Off-axis speckle mode IR holography with high resolution microbolometric sensor

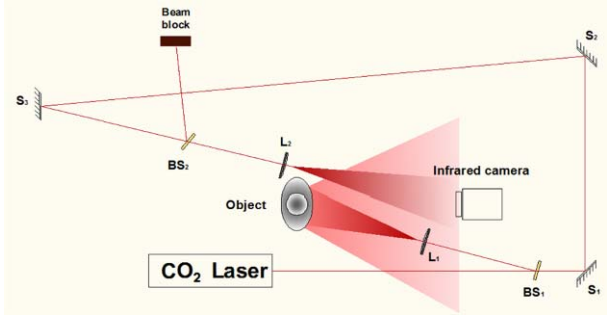

Fig. 10 Off-axis interferometric reflection set-up in reflection mode, S: mirror, L: lens, BS: beam splitter.

Fig. 11 The two small bronzes which were used for testing. One of them (Augustus) was sanded to obtain a different surface finishing

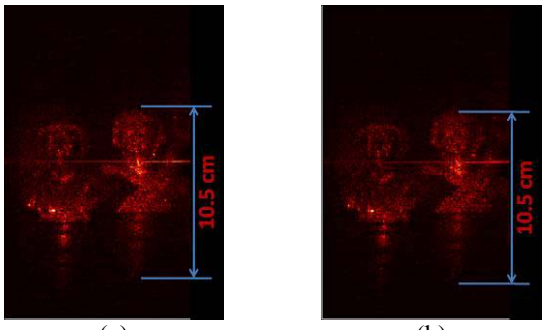

(a) (b)

Fig. 12 (a) Amplitude reconstruction of the two metal objects hologram with Augustus on focus. (b) Amplitude reconstruction of the two metal objects hologram with Traiano on focus.

A more complex configuration, as shown in fig. 10, was tested in order to obtain the amplitude reconstruction of a larger object; in this interferometric set up, the reference beam came from the back of the object so that its direction could be easily adjusted to obtain adequate fringe spacing.

In order to further explore the possibilities offered by this IR DH, we tested the acquisition of objects made of different materials. After a few trials on glass, pottery and marble object, we concentrated our attention on metal items, with different finishing. One of a pair of similar metal objects representing emperors Augustus and Traianus (see fig. 11), was sanded in order to remove the finishing, therefore the quality of the amplitude reconstruction of two objects are noticeably different, as shown in fig. 12.

The two small bronzes were placed at different distances from the detector, with Augustus further away by about 7cm with respect to Traianus, put at a distance of about 22

cm from the detector. Using the appropriate distance in the reconstruction formula, we thus could focus either of the two, as illustrated in fig. 12.

2.5 Interferometer with a larger microbolometric sensor, for off-axis speckle mode IR holography

Another configuration, as described in fig. 13, was used in order to further increase the imaged area. In fact, with the set-up described in fig. 10 when objects with larger dimensions have to be recorded, the recording distance increases up to several meters and this is not feasible in practice.

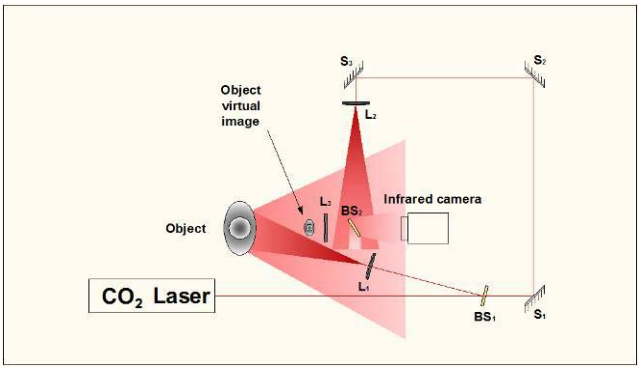

Fig. 13 Off-axis interferometric reflection set-up in reflection mode, with a negative lens, in order to expand the field of view S: mirror, L: lens, BS: beam splitter

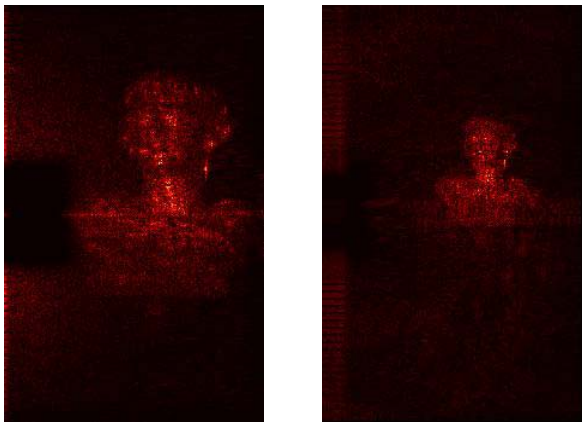

(a) (b)

Fig. 14 (a) Amplitude reconstruction of Augustus hologram with reflection set-up without negative lens (b) Amplitude reconstruction of Augustus hologram with reflection set-up with negative lens.

To reduce the object angle to values with resolvable spatial frequencies spectrum, we prepared an interferometer with a negative lens in the object arm, between the object and the camera, in order to generate a reduced virtual image of the object at a distance b given by the usual lens equation. The wave field emerging from this virtual image is superimposed with the reference wave and the resulting hologram is recorded. As an overall effect we enlarged the field of view of the camera and, by this means, larger object wavefields could be reconstructed. With this configuration we managed to obtain a larger (about 2X) field of view respect to the previous configuration, as shown in fig. 14, and further analyzed in Paragraph. 3.

2.6 Off-axis speckle mode IR double-beam holography with a high resolution pixilated microbolometric sensor

In order to have a more homogeneous distribution of the object beam, the ray was split in two beams, pointing onto two areas, one above the other, along the vertical direction, as illustrated in fig. 15. We also employed a higher resolution camera, an ASi thermal imaging camera (Miricle Thermoteknix 307k, 640x480 detector resolution and 25µm pitch, without the camera's objective). Results are shown in fig. 17.

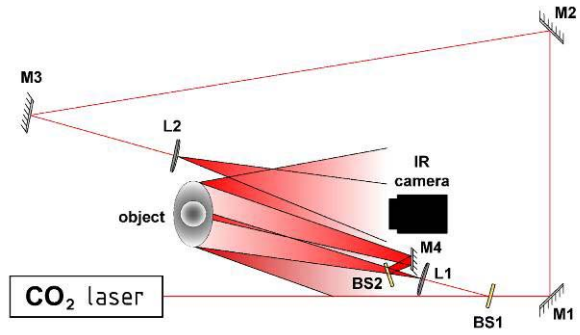

Fig. 15 Off-axis interferometric recording set-up with the object beam split in two S: mirror, L: lens, BS: beam splitter

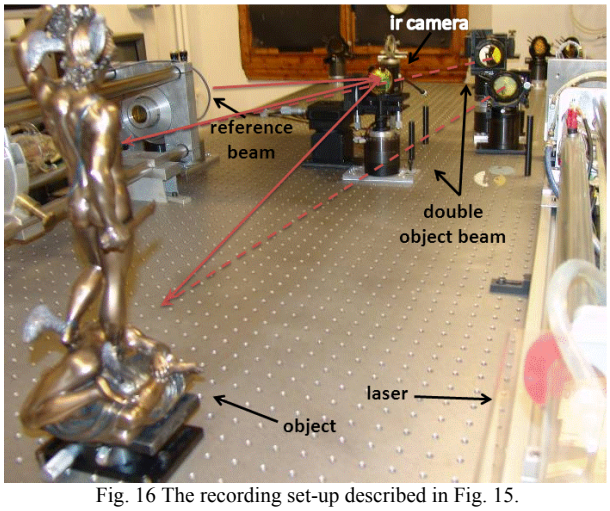

Fig. 16 The recording set-up described in Fig. 15.

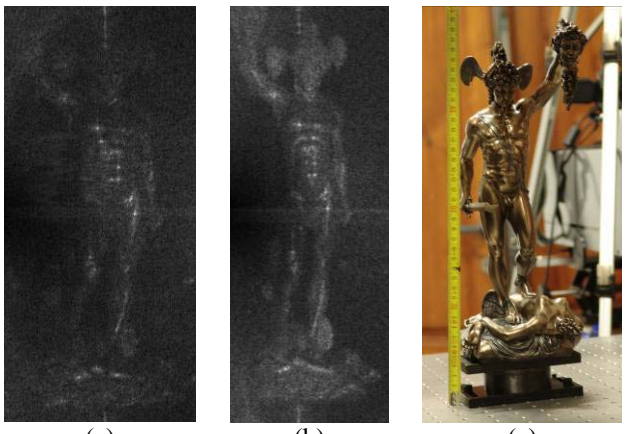

(a) (b) (c)

Fig. 17 (a) Amplitude reconstruction of of the object illustrated in (c) using a single beam, (b) and two beams.

3. Specific considerations for IR digital holographic reconstruction

In order to reconstruct IR holograms, a number of critical aspects occurring in DH have to be taken into account. The digital recording and reconstruction process of hologram has in fact an important drawback compared with its analog counterpart, which is the general lack of resolution of digital recording devices compared to films, this is crucial especially for the IR range, since the available sensors have a rather limited number of active pixels.

In order to satisfy the Whittaker-Shannon sampling theorem, the fringe period of the interference pattern P has to satisfy the following inequality:

$$P = \frac{\lambda}{2\sin(\theta/2)} \geq 2d_p \tag{2}$$

which establishes that the fringe period P has to be larger than two times the detector pixel pitch d_p, where θ is the angle between the reference and the object beam.

This limitation fixes a maximum value for θ, which considering small values of it, reduces to lambda over two times the pixel pitch (equation 3).

$$\theta_{\max} = 2\sin^{-1}\left(\frac{\lambda}{4d_p}\right) \overset{small\ angles}{\approx} \frac{\lambda}{2d_p} \tag{3}$$

It is thus remarkable that θ presents an inverse proportionality to d_p and a direct proportionality to the wavelength λ. From this maximum value of θ, it follows that a minimum distance value between the object and the detector can be assessed.

In the in-line configuration, the maximum angle and the minimum distance dmin can be easily computed by geometrical considerations.

$$d_{\min} = \frac{d_p\left(D + Nd_p\right)}{\lambda} \overset{D>>Nd_p}{\approx} \frac{d_p D}{\lambda} \tag{4}$$

where D is the object lateral size and N the number of the sensor pixels.

In particular, for objects larger than the CCD lateral dimension, Nd_p, the expression for the minimum distance further simplifies as indicated in (equation 4), from which we can infer that this value is in inverse proportion to the wavelength λ used, and in direct proportion to the pixel pitch d_p.

Considering that we are working in Fresnel approximation, we can assume our computation essentially reduces to a discrete Fourier Transform. Then the resolution of the reconstructed image, along the two axes, shows proportionality to the reconstruction distance and to the wavelength in use.

$$\Delta x_R = \frac{\lambda d}{N\Delta x_H} \quad \Delta y_R = \frac{\lambda d}{N\Delta y_H} \tag{5}$$

where d is the distance of the object from the camera, and Δx_H and Δy_H are respectively the horizontal and the vertical dimension of the camera pixel. If, for simplicity, we consider to have a square detector with square pixels, where $\Delta x_H = \Delta y_H = d_p$ and we further assume to record the hologram at the minimum distance allowed by the sampling theorem, the resolution pixel approaches its minimum value and becomes independent from the wavelength in use.

$$\Delta x_R = \Delta y_R = \frac{D + Nd_p}{N} \overset{D>>Nd_p}{\approx} \frac{D}{N} \tag{6}$$

Besides, for large objects, the expression further simplifies and becomes dependent only on the object dimension and the CCD elements (equation 6).

We can therefore infer that despite the important drawback connected with the current dimensions of the thermal camera pixels, the use of longer wavelengths in digital holography has several advantages, especially in the hologram recording of large objects: first of all the stability of the system becomes a less critical factor at longer wavelengths, secondly, as one can see from the previous expressions, the angle θ between the reference beam and the object beam, increases with the wavelength and consequently the distance between the camera and the object can be reduced to more acceptable laboratory values even for large objects (see fig. 18). Moreover, with CO_2 lasers is possible to reach very high power outputs and this makes it easier to expand the beam and irradiate large objects. Besides, as we previously described, the resolution of the reconstruction image at the minimum distance, is not influenced by the wavelength in use.

In order to further increase the size of achievable objects we tested also a different configuration, using a concave lens, as suggested by Pelagotti et al 2009. With this set-up, shown in fig. 19, the wave-field reflected from the object's surface is drastically reduced because it emerges from the small virtual image of the object created by the lens and not from the large object itself. While the angle between rays from edge points of the large object and the normally impinging plane reference wave is too large to satisfy the sampling theorem, the angle θ between rays coming from the virtual object and the reference wave is much smaller so that it meets the requirements of equation (2).

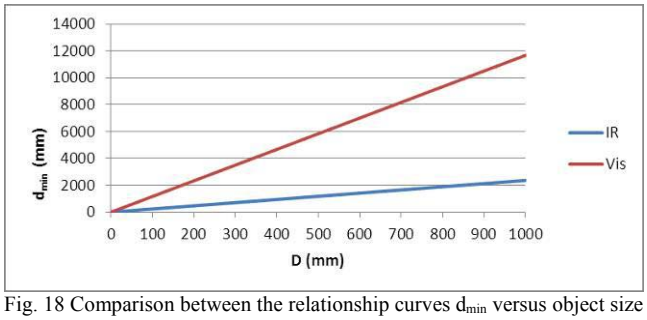

Fig. 18 Comparison between the relationship curves d_{min} versus object size for the thermocamera (blu line) with 640x 480 pixels, pixel size Δx = 25 µm, and λ=10.6 µm and for a typical visible CCD sensor (red line) with 1024x 1024 pixels, pixel size Δx = 11 µm, and λ=0.6328 µm.

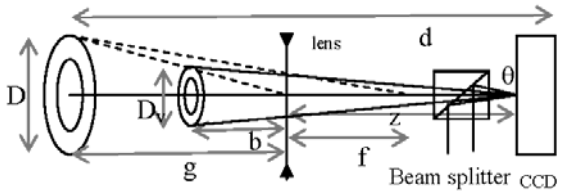

Fig. 19 Schematics of a recording set-up with a negative lens

Using a lens with negative focal length we can calculate the distance z that the lens must have from the camera and the distance g between object and lens. The calculation is

based on the lens formula and on the magnification formula.

$$M_T = \frac{D_V}{d} = -\frac{f}{g-f} \tag{7}$$

Here M_T denotes the transversal magnification, D_V is the lateral extension of the virtual image. With:

$$\tan\theta = \frac{D_V}{2(z+b)},\ D_V = -\frac{df}{g-f}, b = \frac{gf}{f-g} \tag{8}$$

we obtain

$$z = -\frac{D\ f}{(g.f)^2 \tan\theta} + \frac{fg}{g-f} \tag{9}$$

The object size is reduced by the magnification factor M_T but the distances b between the virtual images and the lens are not reduced by the same factor. For them the longitudinal magnification factor M_L applies which is a consequence of the lens formula. We have $M_L = -M_T^2$. The minus sign accounts for the reversal of the position order.

4. Holography Display with visible wavelength of digital hologram recorded at IR: comparison by means of synthetic aperture

In order to compare results of IR recorded holograms and visible recorded holograms, we stitched together 4 holograms recorded with a thermal camera, acquired shifting the camera twice horizontally and vertically. This technique allows to synthetically increase the numerical aperture and to get a number of recording pixels similar to that of the visible sensors (Paturzo et al 2008 , Paturzo et al 2009). As expected, after processing the synthetic hologram, which results a 1146x834 pixel image, an inverse Fresnel transformation provides an enhanced resolution reconstruction, compared with what is achievable with a single hologram, (compare fig. 12 and 21(c)) and resolution of the reconstruction of the IR hologram similar to that of the visible hologram (compare fig. 20 (c) and fig. 22 (c).

5. Real-time optical reconstruction at visible wavelength of IR recorded holograms

In this last experiment (Paturzo et al 2010), our aim was to use the system described in fig. 10 to acquire large object holograms and integrate the recording step with a reconstruction and display process. In the reconstruction process, we use a DPSS laser emitting at 0.532 μm. The laser beam is expanded so to obtain a convergent beam that impinges on an Spatial Light Modulator (SLM) and displays the recorded hologram. An image is produced to a certain distance from the SLM and, e.g., can then be acquired by a CCD camera.

Generally, when an hologram is reconstructed with a different wavelength from the one used in the recording process, the image obtained is affected by aberrations and distortions, which depend on the two wavelength ratio and the difference in the pixel pitch. However, thanks to the digital nature of the hologram data that we acquired, we could easily apply to the data linear and non-linear stretching, as well as scale-change (Paturzo and Ferraro 2009), while with an appropriate configuration, aberrations such as e.g. coma or astigmatism, are demonstrated to be rather insignificant.

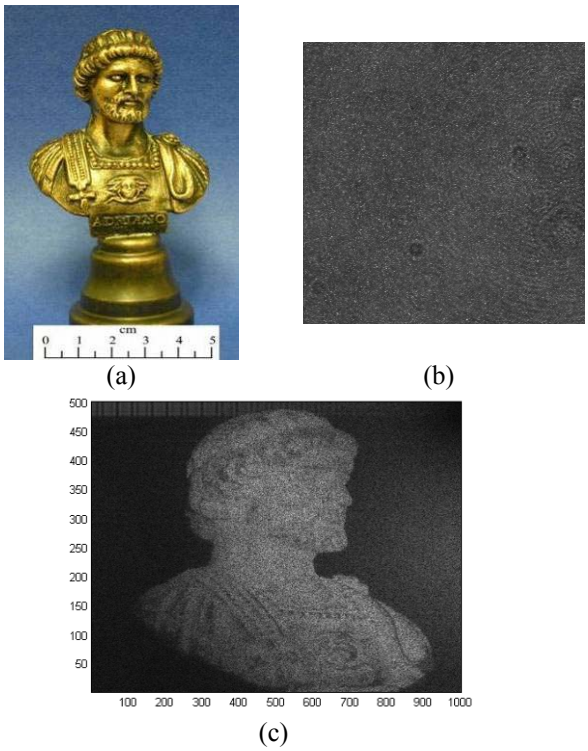

(a) (b) (c)

Fig. 20 (a) A small bronze used for testing in the visible range; (b) A 1024x1024 speckle hologram acquired with a CCD camera in the visible range, λ=0.6 μm; (c) its amplitude reconstruction.

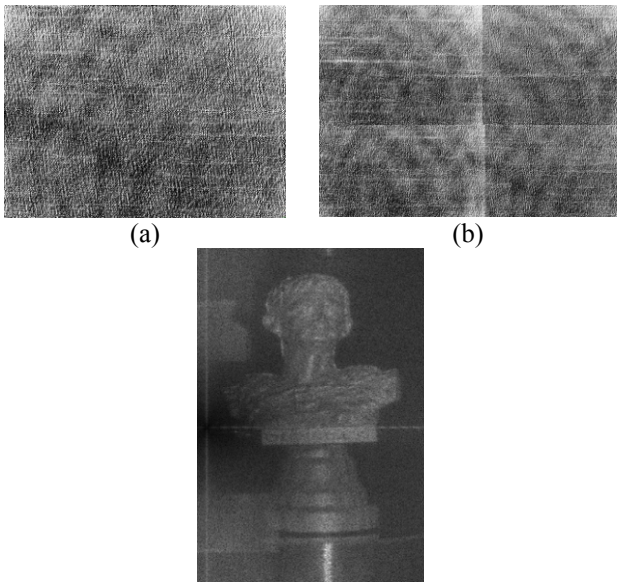

(a) (b) (c)

Fig. 21 (a) A 640x480 speckle hologram acquired with a CCD camera in the IR range, λ=10.6 μm of the small bronze Augustus of Fig. 11(b) Mosaic of 4 IR 640x480 holograms, acquired at shifted camera positions, both horizontally and vertically. The resulting hologram is a 1146x834 pixel image. (c) Amplitude reconstruction of the mosaic hologram.

Moreover, the set-up that integrates the recording and displaying unit, has the major advantage to allow a quasi-real-time direct access to 3D optical imaging in the visible

spectrum of holograms recorded at long IR (see fig. 22). In the recording process, we used the coherent light source produced the same laser as described in Paragraph 2.3. The laser beam was set on the fundamental TEM00 mode at about 110 W of emission power.

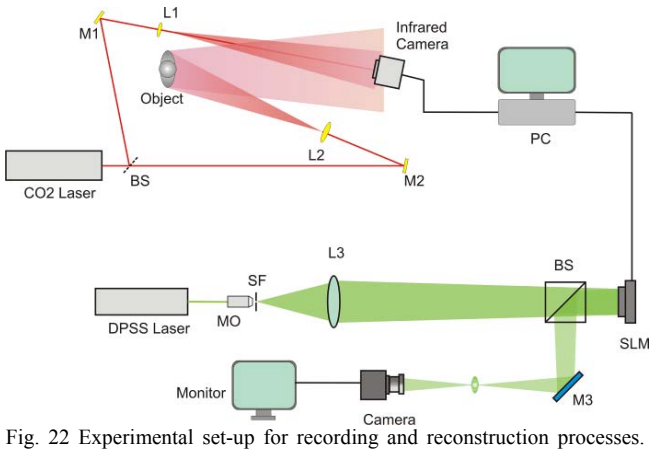

Fig. 22 Experimental set-up for recording and reconstruction processes. M: mirror, L: lens, BS: beam splitter, MO: microscope objective, SLM: spatial light modulator, SF: spatial filter

In these conditions the laser beam is characterized by a waist of 10 mm and a divergence of 2 mrad. The hologram was recorded by means of the same camera described in Paragraph 2.3. Even in this case, the numerical reconstruction of object wavefront amplitude was executed according to the discretization of the Fresnel approximation of Rayleigh Sommerfeld equation.

As far as the aberrations of the reconstructed images, are concerned, according to Meyer's theory (Meier 1965) the Fourier configuration is specially suitable, since it allows them to be minimized.

We computed the lateral magnification and found that its value results different from identity. In the Fourier configuration holography the lateral magnification is expressed by the formula:

$$M_{lat} = \frac{1}{m}\frac{\lambda_c}{\lambda_r}\frac{z_i}{z_o} \tag{10}$$

where m is scale-change factor of the hologram, λ_r and λ_c are the wavelengths of the recording (10.6 μm, CO_2 laser) and reconstruction (532nm, green laser) set-up, respectively, while z_i and z_o are the distance of the image and the object from the hologram plane. To estimate the magnification we need to calculate the distance at which the reconstructed image appears in focus. The position of the image is obtained by the formula:

$$\frac{1}{z_i} = \frac{1}{z_c} \pm \frac{1}{m^2}\frac{\lambda_c}{\lambda_r}\left(\frac{1}{z_0} - \frac{1}{z_r}\right) \tag{11}$$

We note that, for a Fourier hologram (z_o=z_r), z_i has the same value of the radius of curvature of the reconstructing beam z_c and does not depend on the wavelength ratio and on the scale-change factor of the hologram, m. This is confirmed by the experiment performed in (Paturzo and Ferraro 2009), where it is demonstrated that the linear stretching of Fourier holograms doesn't produce a change in the in-focus reconstruction distance as, instead, it happens for Fresnel holograms.

Considering that the parameters used in our experiment are λ_r = 10.6 μm, λ_c = 0.532 μm, m=8/35, z_c = 80 cm, z_o=z_r=50 cm, M_{lat} results equal to 0.36, in agreement with measured value.

As to the wavefront aberrations, we consider the Seidel aberration formula in polar coordinates.

The spherical aberration is zero for hologram acquired in Fourier configuration, regardless of the magnitude of z_c, λ_r, λ_c and m.

The coma aberration is given by

$$W = \left(\frac{2\pi}{\lambda_c}\right)\left[\frac{1}{2}\rho^3\left(C_x\cos\theta + C_y\sin\theta\right)\right] \tag{12}$$

while the astigmatism is expressed by the formula

$$W = \left(\frac{2\pi}{\lambda_c}\right)\left[-\frac{1}{2}\rho^2\begin{pmatrix}A_x\cos^2\theta + A_y\sin^2\theta \\ +2A_{xy}\cos\theta\sin\theta\end{pmatrix}\right] \tag{13}$$

The field of curvature is

$$W = \left(\frac{2\pi}{\lambda_c}\right)\left[-\frac{1}{4}\rho^2 F\right] \tag{14}$$

while the distortion is given by

$$W = \left(\frac{2\pi}{\lambda_c}\right)\left[\frac{1}{2}\rho\left(D_x\cos\theta + D_y\sin\theta\right)\right] \tag{15}$$

For holograms acquired in Fourier configuration,

$$C_x = \frac{\mu}{m}\left[-\frac{x_0}{z_0}\left(\frac{1}{m^2 z_0^2} - \frac{1}{z_c^2}\right) + \frac{x_r}{z_r}\left(\frac{1}{m^2 z_0^2} - \frac{1}{z_c^2}\right)\right] \tag{16}$$

$$A_x = \frac{\mu}{m^2}\left[-\frac{x_0^2}{z_0^2}\left(\frac{1}{z_0} + \frac{\mu}{z_c}\right) + \frac{x_r^2}{z_r^2}\left(\frac{1}{z_0} + \frac{\mu}{z_c}\right)\right] \tag{17}$$

where the ratios x_o/z_o and x_r/z_r remain finite and they are equal to the tangents of the off-axis angles of both beams.

$$F = \frac{x_c^2 + y_c^2}{z_c^3} - \frac{\mu\left(x_o^2 + y_o^2\right)}{m^2 z_o^3} + \frac{\mu\left(x_r^2 + y_r^2\right)}{m^2 z_r^3} - \frac{a_i^2 + b_i^2}{z_i^3} \tag{18}$$

where z_i is the position and a_i and b_i the off-axis coordinates of the real image.

In our experiment, x_r/z_r and x_c/z_c are equal to zero, this means that the reference beams in the recording and in reconstruction processes are normal to the CCD camera and SLM, respectively.

This experimental condition leads also to a simplified formula for the distortion coefficient, that, therefore, is given by

$$D_x = \frac{\mu}{m}\left(\frac{x_0^3 + x_0 y_0^2}{z_0^3}\right)\left(\frac{\mu^2}{m^2} - 1\right) \tag{19}$$

Inserting the experimental parameters in the eq. (6-10), the coefficients values result to be

$$C_x = -1.8 * 10^{-6}\, mm^{-2}$$

$$A_x = -2.2*10^{-5}\,mm^{-1} \quad (20)$$
$$F = -2.3*10^{-5}\,mm^{-1}$$
$$D_x = -2.8*10^{-4}$$

The lateral dimensions of SLM are such that ρ = 1.5 mm, therefore coma results about 6/1000 λ, astigmatism 5/100 λ, field of curvature 3/100 λ and distortion 4/10 λ.

Consequently, we can assert that, in our experimental conditions, the wavefront aberration is negligible (lower than 1 wavelength) and, therefore, doesn't substantially affect the reconstructed images, therefore granting the possibility of an accurate IR/recording-VIS/reconstruction holographic system.

Fig. 23 A spectator observing the acquired holograms SLM optical reconstructions, projected on a screen. The size of the image reconstructed at visible wavelength was about 30 cm, comparable to the original object size

6. Conclusions

Recent availability of digital thermal cameras with larger sensors, paved the way to the extension of DH in the infrared radiation range.

This band offers interesting possibilities in crucial applications such as homeland security, night vision and biological science.

We presented the pioneering activities of our laboratory in testing digital holography at 10.6 µm, both in transmission and reflection configurations. Thanks to the long wavelength involved, we managed to reconstruct various size objects: from less than 1 mm to about 40 cm. We also tested the possibilities offered by this technique with various materials.

We compared the results of infrared holography with those in the visible range, increasing the numerical aperture (N.A.) of an IR sensor in with a synthetic aperture approach.

Moreover, we performed optical reconstruction of digital holograms recorded at long IR wavelength by means of a Spatial Light Modulator at 532nm. The integrated recording and reconstruction process is demonstrated by a configuration that minimizes aberrations.

Acknowledgements

The research leading to these results has received funding from the European Community's Seventh Framework Programme FP7/2007-2013 under grant agreement n° 216105 ("Real 3D" Project).

References

1. E. Allaria, S. Brugioni, S. De Nicola, P. Ferraro, S. Grilli, R. Meucci, (2003) Digital holography at 10.6 micron, *Opt. Commun*. **215**:257–262
2. R. Beaulieu, R. A. Lessard, M. Cormier, M. Blanchard, M. Rioux, (1978) Pulsed ir holography on Takiwax films. *Appl. Opt*. **17**:3619
3. R. M. Beaulieu, R. A. Lessard (1997) Review of recording media for holography at 10.6 µm, *Proc. SPIE*. **30112**:98-305
4. S. Calixto (1988) Infrared recording with gelatin films. *Appl. Opt*. **27**:1977-1983
5. J. S. Chivian, R. N. Claytor, D. D. Eden (1969) Infrared holography at 10.6 µm. *Appl. Phys. Lett*. **15**:123-125
6. G. Decker et al (1972) Holography and Holographic interferometry with pulsed high-power lasers. *Appl. Phys. Lett*. **20**:490
7. S. De Nicola, P. Ferraro, S. Grilli, L. Miccio, R. Meucci, P. K. Buah-Bassuah, F. T. Arecchi (2008) Infrared digital reflective-holographic 3D shape measurements. *Opt. Commun*. **281**:1445–1449
8. P. Ferraro, S. De Nicola, A. Finizio, G. Coppola, S. Grilli, C. Magro, G. Pierattini (2003) Compensation of the inherent wave front curvature in digital holographic coherent microscopy for quantitative phase-contrast imaging. *Appl. Opt*. **42**:1938–1946
9. P. Ferraro, S. De Nicola, A. Finizio, G. Pierattini, G. Coppola (2004) Recovering image resolution in reconstructing digital off-axis holograms by Fresnel-transform method. *Applied Physics Letters*. **85**:2709-2711
10. P. Ferraro, S. Grilli, D. Alfieri, S. De Nicola, A. Finizio, G. Pierattini, B. Javidi, G. Coppola, V. Striano (2005) Extended focused image in microscopy by digital holography. *Opt. Express*. **13**:6738–6749
11. P. Ferraro, M. Paturzo, P. Memmolo, A. Finizio (2009) Controlling depth of focus in 3D image reconstructions by flexible and adaptive deformation of digital holograms. *Opt. Lett*. **34**:2787–2789
12. S. Grilli, P. Ferraro, S. De Nicola, A. Finizio, G. Pierattini, R. Meucci (2001) Whole optical wavefields reconstruction by digital holography. *Opt. Express*. **9**: 294–302
13. R. W. Meier (1965) "Magnification and Third-Order Aberrations in Holography," J. *Opt. Soc. Am*. **55**:987-992
14. M. Paturzo, F. Merola, S. Grilli, S. De Nicola, A. Finizio, P. Ferraro (2008) Super-resolution in digital holography by a two dimensional dynamic phase grating. *Optics Express*. **16**:17107- 17118

15. M. Paturzo, P. Ferraro (2009) Correct self-assembling of spatial frequencies in super-resolution synthetic aperture digital holography. *Opt. Lett*. **24**:3650- 3652
16. M. Paturzo, P. Ferraro (2009) "Creating an extended focus image of a tilted object in Fourier digital holography," *Opt. Express*. **17**:20546-20552
17. M. Paturzo, A. Pelagotti, A. Finizio, L. Miccio, M. Locatelli, A. Gertrude, P. Poggi, R. Meucci, P. Ferraro (2010) Optical reconstruction of digital holograms recorded at 10.6 μm: route for 3D imaging at long infrared wavelengths. *Opt. Lett*. **35**:2112-2114
18. A. Pelagotti, M. Locatelli, A. Gertrude, P. Poggi, R. Meucci, M. Paturzo, L. Miccio, P. Ferraro "Reliability of 3D imaging by digital holography at long IR wavelength" *IEEE/OSA Journal of Display Technology (in press).*
19. D. Prévost, G. Thibault, P. Galarneau, M. Denariez-Roberge, A. Tarrats-Saugnac, F. de Contencin (1989) Thermal gratings written in glycerol with CO2 laser radiation. *Appl. Opt*. **28**:3751-3753
20. L. Repetto, R. Chittofrati, E. Piano, C. Pontiggia (2005) Infrared lensless holographic microscope with a vidicon camera for inspection of metallic evaporations on silicon wafers. *Opt. Comm*. **251**:44-50
21. M. Rioux, M. Blanchard, M. Cormier, R. Beaulieu, D. Bélanger (1997) Plastic recording media for holography at 10.6 μm. *Appl. Opt*. **16**:1876-1879
22. M. Rioux, M. Blanchard, M. Cormier, R. Beaulieu (1978) Use of the TEM10 laser mode for ir holography at 10.6 μm *Appl. Opt*. **17**:3864
23. G. I. Rukman, B. E. Lisyanskii, P. A. Morozov, S. P. Morozova, (1978) Holography in the IR region of the spectrum, based on scanning image converters. *Meas. Techniques*. **21**:635–636
24. T. Sakusabe, S. Kobayashi (1971) Infrared Holography with Liquid Crystals. Jpn. J. Appl. Phys. **10**:758-761
25. K. Shigeaki, K. Kyoko (1971) Infrared Holography with Wax and Gelatin Film. *Appl. Phys. Lett*. **19**:482
26. A. Stadelmaier, J. H. Massig (2000) Compensation of lens aberrations in digital holography. *Opt. Lett*. **25**:1630-1632